Sensor and Simulation Notes

Note 229

September 1977

Field Distributions on a Two-Conical-Plate and a Curved Cylindrical-Plate Transmission Line

F.C. Yang
Lennart Marin

Dikewood Corporation, Westwood Research Branch
Los Angeles, California

Abstract

The method of stereographic projection is used to reduce the problem of calculating the TEM field distribution on two conical plates to the problem of determining the TEM field distribution on two cylindrical plates of circular arc. The curved-cylindrical-plate problem is solved by the method of conformal mapping. Graphs are presented for the field lines and field distributions of the TEM modes on both the conical and cylindrical transmission lines for various cone angles and plate widths.

ACKNOWLEDGEMENT

Thanks go to Drs. C.E. Baum, J.P. Castillo, and K.C. Chen of the Air Force Weapons Laboratory for many enlightening discussions.

SECTION I
INTRODUCTION

The working volume of most bounded-wave simulators consists of the forward region between two parallel plates (figure 1). The desired electromagnetic field in the working volume is established by launching a pulser-generated transient wave on conical-plate wave launchers. To avoid unwanted reflections from the passive end of the simulator the two parallel plates are terminated by a conical-plate termination section. Test objects such as aircraft and missiles are placed in the simulator's working volume during tests.

To analyze the electromagnetic field in the working volume it is necessary to know the field distribution of the TEM mode both on the parallel plates and on the conical plates. The TEM mode on two finite-width, parallel plates have been studied in great detail (refs. 1, 2, and 3). In all these references the method of conformal mapping is used, the actual transformation being identical to that derived in ref. 4.

The characteristic impedance of the TEM mode on two conical plates is investigated in ref. 5 for a wide variety of cone angles and plate widths. The TEM mode impedance for the special case where both conical plates are located in the same plane is also calculated in refs. 6 and 7. In this report we continue the investigation of the TEM mode on two conical plates and present results for the distribution of its electric and magnetic fields. In the course of finding this field distribution we also determine the field distribution of the TEM mode on two cylindrical plates of circular arc. It should be mentioned that an investigation is given in refs. 8 and 9 of certain properties of the field generated in the parallel-plate section of a bounded-wave simulator by a pulse launched in the conical feeding section.

In section II we briefly repeat (1) the stereographic projection used in ref. 5 to project the conical plates onto two cylindrical plates of circular arc and (2) the conformal mapping used to map the curved plates to a simple structure whose TEM mode field distribution is well known. The conformal mapping is then used in section III to find both the electric and magnetic field lines as well as the spatial variation of the field strength of the TEM mode on the cylindrical line. Finally, in section IV, we stereographically project the field distribution of the TEM mode on the cylindrical line to obtain the electric and magnetic fields of the TEM mode on the conical line.

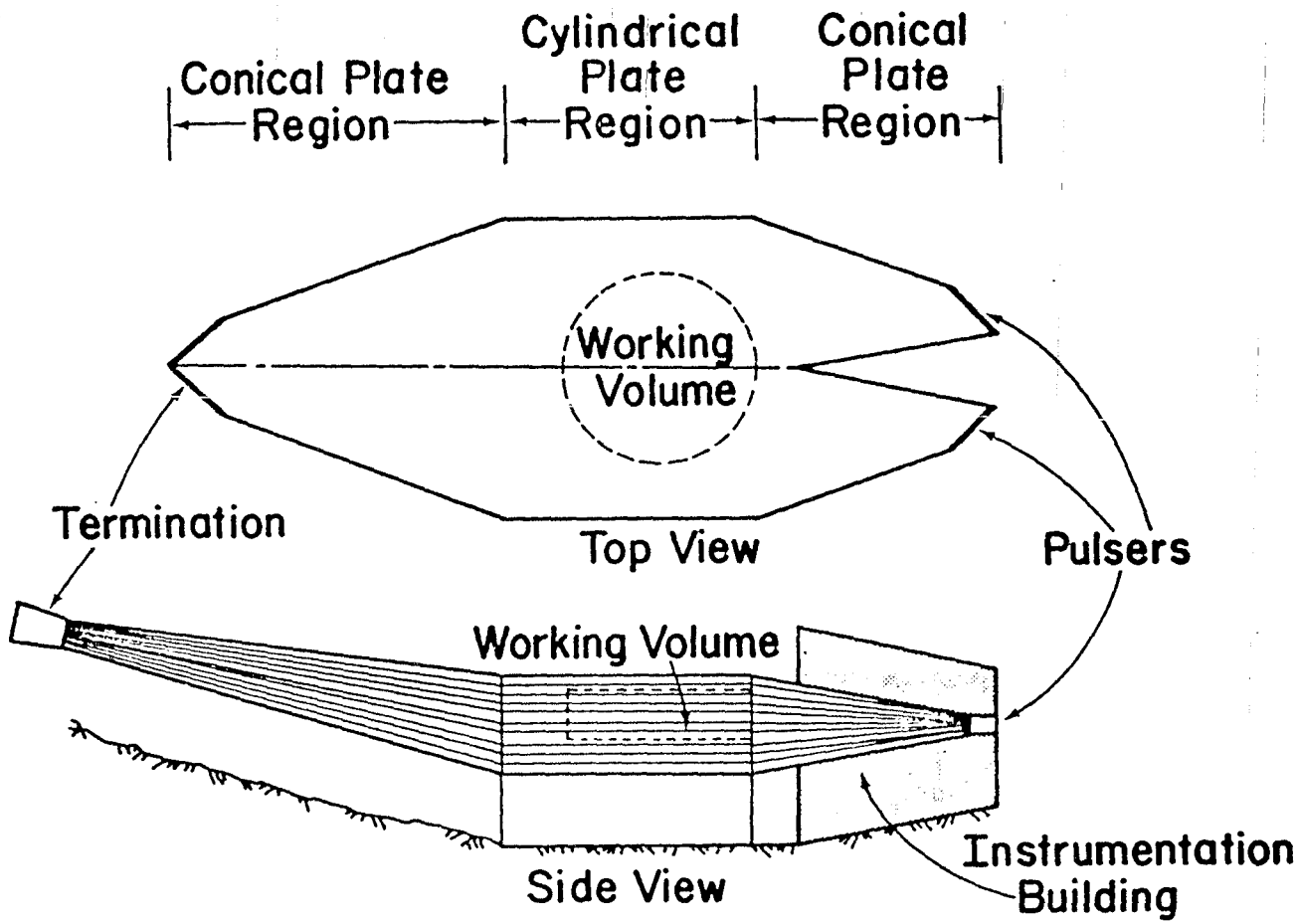

Figure 1. Top and side views of a bounded-wave simulator.

SECTION II

THE STEREOGRAPHIC PROJECTION AND CONFORMAL TRANSFORMATION

To analyze the field distribution of the TEM mode on the two conical plates the methods of stereographic projection and conformal mapping are used in ref. 5. The geometry of two conical plates is shown in 2, whereas the projection procedure is shown in figure 3. In this procedure, a point (x,y,ℓ) in the $z = \ell$ plane is first projected onto the point (x'',y'',z'') on the surface of a sphere with radius ℓ and center at the origin (the apex of the two conical plates, see figure 4). The point (x'',y'',z'') is then stereographically projected back onto the point (x',y',ℓ) as shown in figure 3. It is easy to see that the mapping of points (x,y) to points (x',y') is a one-to-one mapping that maps the entire $z = \ell$ plane onto the interior of a circle with radius 2ℓ and center at $(0,0,\ell)$. In fact, we have

$$x' = \frac{2x\ell}{\ell + \sqrt{\ell^2 + x^2 + y^2}} \qquad (1)$$

$$y' = \frac{2y\ell}{\ell + \sqrt{\ell^2 + x^2 + y^2}} \quad .$$

It is also shown in ref. 5 that the stereographic projection maps the two conical plates onto the two plates of circular arc (figure 5). In the special case where $\theta_o = 90°$ then the centers of the two circles both are located at the origin of the x',y' plane. This case has been treated in ref. 10.

By considering the x',y' plane as the complex z' plane it is shown in ref. 5 that the first quadrant of the x',y' plane can be conformally mapped into the shaded region of the W plane shown in figure 6. In figures 5 and 6 we also indicate how certain points A, B, C, D, E are mapped by the conformal transformation. The complex W plane can be interpreted as a complex potential plane where $V_o/2$ is the potential of the plate BCD. Since the equipotential lines map conformally this means that the potential on the upper plate of circular arc of figure 5 is also $V_o/2$.

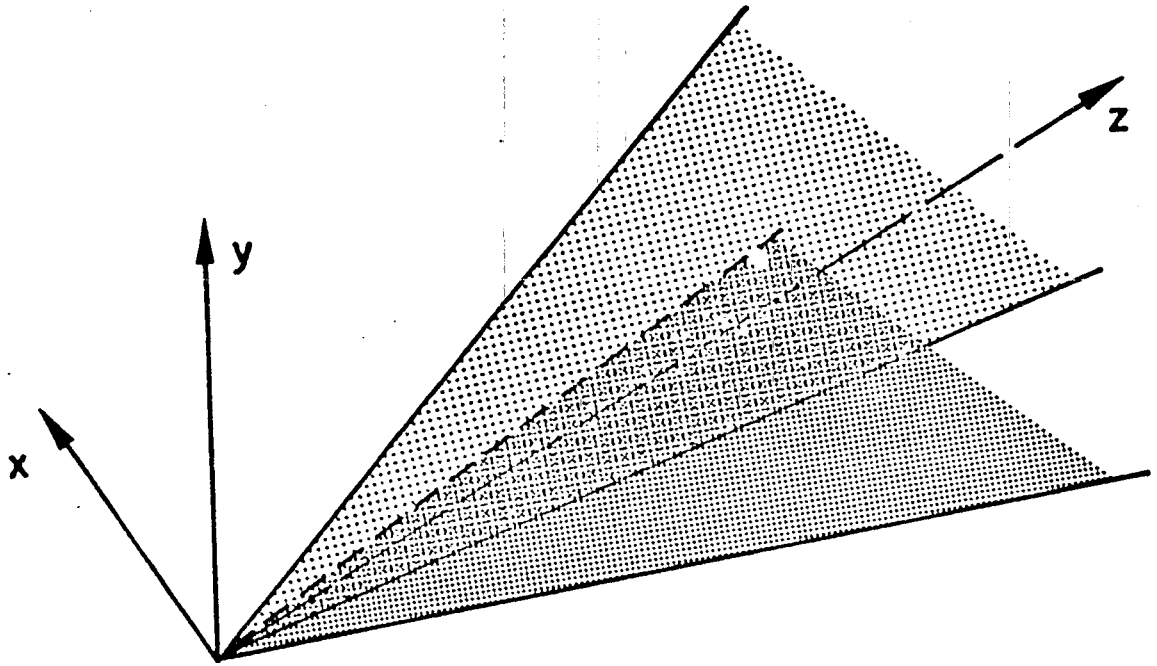

Figure 2. Two conical plates.

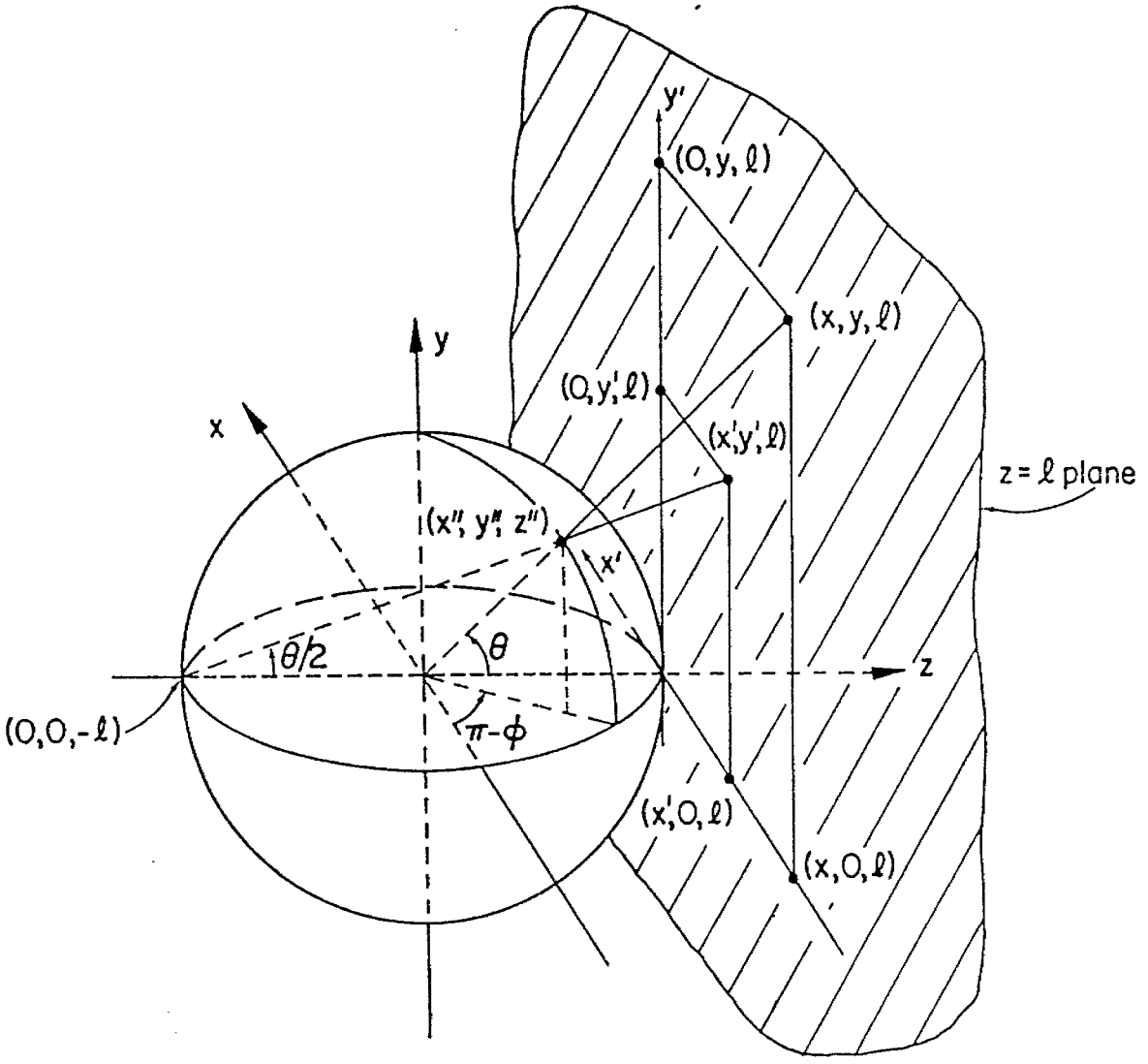

Figure 3. Projection of (x,y) to (x',y').

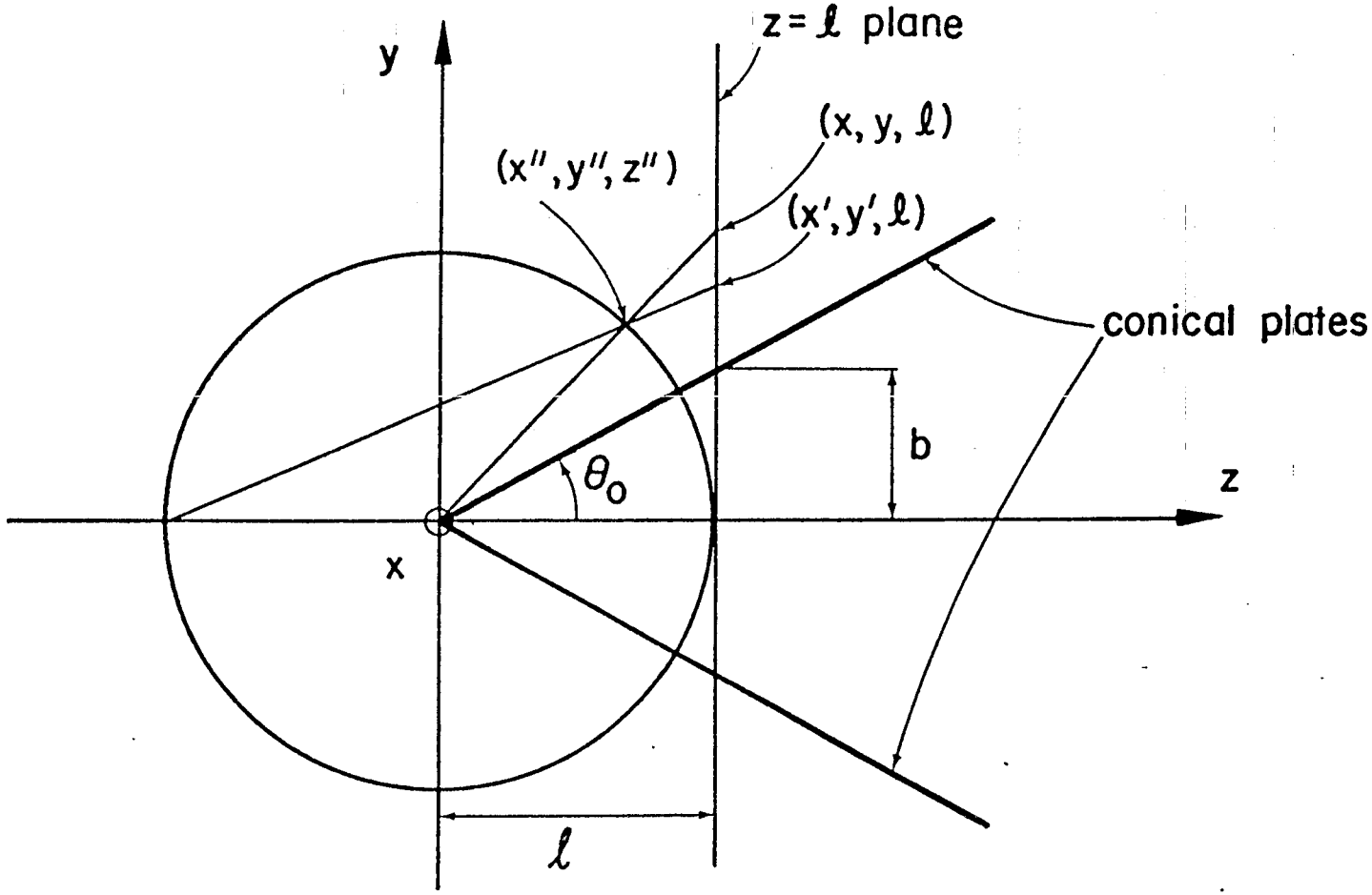

Figure 4. Planar view of stereographic projection in figure 3 including cross section of conical plates.

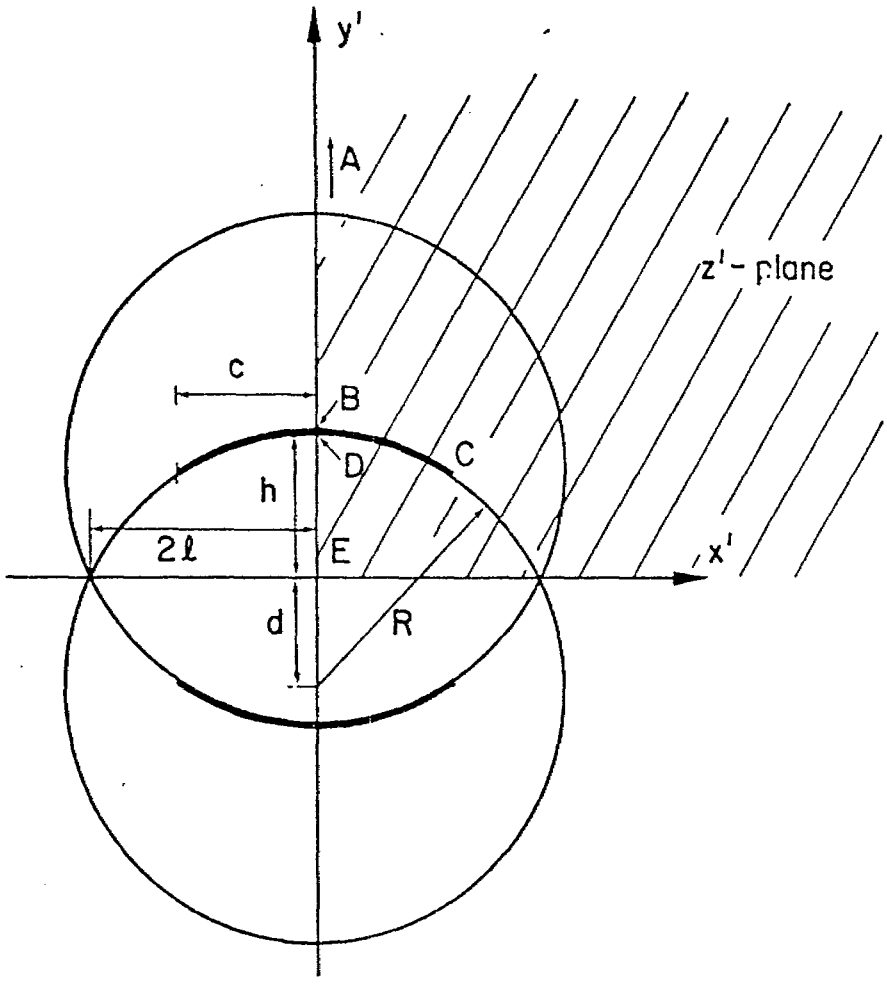

$$R = (2\ell/b)\sqrt{b^2+\ell^2}$$

$$d = 2\ell^2/b$$

$$h = R-d$$

$$c = 2a\ell/(\sqrt{a^2+b^2+\ell^2}+\ell)$$

Figure 5. Stereographic projection of two conical plates onto two plates of circular arc.

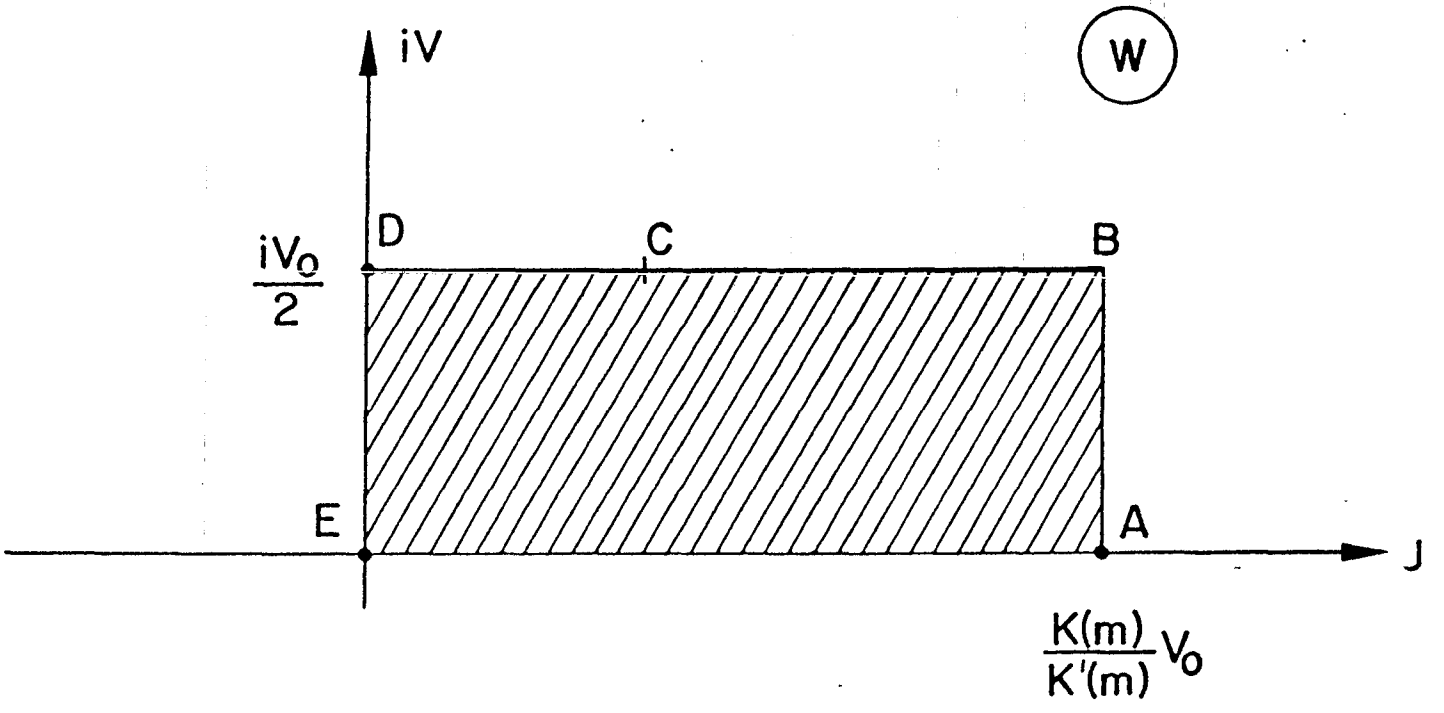

Figure 6. Image of the first quadrant of the complex z' plane under the conformal mapping 2).

The mathematical details of the transformation that conformally maps the shaded region of the z'-plane in figure 5 to the shaded region of the W-plane are derived in ref. 5. We therefore do not repeat the steps leading up to this transformation, but merely mention that the relationship between points $z' = x' + iy'$ and points $W = U + iV$ can be expressed implicitly in the following manner

$$z' = 2\ell \tanh(z_1/2)$$

$$z_1 = -\sqrt{(1-n)(m-n)/n}\ \left[uA_1^{-1} - \Pi(n;\, u|m) + \sqrt{n}\, f(m,n,u)\right] + i\theta_o$$

$$f(m,n,u) = \frac{1}{2\sqrt{(1-n)(m-n)}}\, \ell n\left[\frac{2(1-n)(m-n) + (1 - n\,sn^2(u))(n+nm-2m)}{n(m-1)[1 - n\,sn^2(u)]} + \frac{2n\sqrt{(1-n)(m-n)}\ cn(u)dn(u)}{n(m-1)[1 - n\,sn^2(u)]}\right] \qquad (2)$$

$$u = -2K'(m)W(z')/V_o + K(m) + iK'(m)$$

where $\Pi(n;\, u|m)$ is the incomplete elliptic integral of the third kind and m, n, A_1 are solutions of (12) in ref. 5.

From the set of equations (2) we can determine the transverse variation of the stream function $U(x',y')$ and the potential function $V(x',y')$, and consequently also the electromagnetic field distribution of the TEM mode on the curved plates. With the aid of the stereographic projection relationship (1) we then determine the field distribution of the TEM mode on the conical plates.

SECTION III

TEM-MODE FIELD DISTRIBUTION ON TWO PLATES OF CIRCULAR ARC

1. *Electric and Magnetic Field Lines*

It is well known that the electric field lines are identical to the stream lines (U = const.) of the complex potential function W(z') and that the magnetic field lines are identical to the equipotential lines (V = const.). In figure 7 we show the equipotential lines and stream lines for three different plate configurations (only the first quadrant is included for symmetry reasons). The potential change between two consecutive equipotential lines is $V_o/20$ and change of the stream function between two consecutive stream lines is $[K(m)/K'(m)]V_o/10$. The directions of the corresponding electric and magnetic field lines are also indicated in figure 7.

2. *Electric and Magnetic Field Strengths*

The electric and magnetic field distributions of the TEM mode can be obtained from the derivative of W(z') in the following way:

$$\begin{aligned}
\frac{dW}{dz'} &= \frac{\partial U}{\partial x'} + i\,\frac{\partial V}{\partial x'} \\
&= \frac{\partial V}{\partial y'} + i\,\frac{\partial V}{\partial x'} = -E'_y - iE'_x \\
&= \frac{\partial U}{\partial x'} - i\,\frac{\partial U}{\partial y'} = (H'_x - iH'_y)Z_o \\
&= \frac{1+t\sqrt{n}}{1+t\sqrt{n}-A_1}\,\frac{1}{1-(z'/2\ell)^2}\,\frac{A_1\sqrt{n}}{K'(m)\sqrt{(1-n)(m-n)}}\,\frac{2h}{\sqrt{R^2-d^2}}\,\frac{V_o}{2h}
\end{aligned} \tag{3}$$

where $t = sn(u)$ and where we have made use of the Cauchy-Riemann relationships for harmonic functions. Equations (2) and (3) together give the electric and magnetic fields of the TEM mode at an arbitrary point (x',y') in the plane transverse to the curved plates.

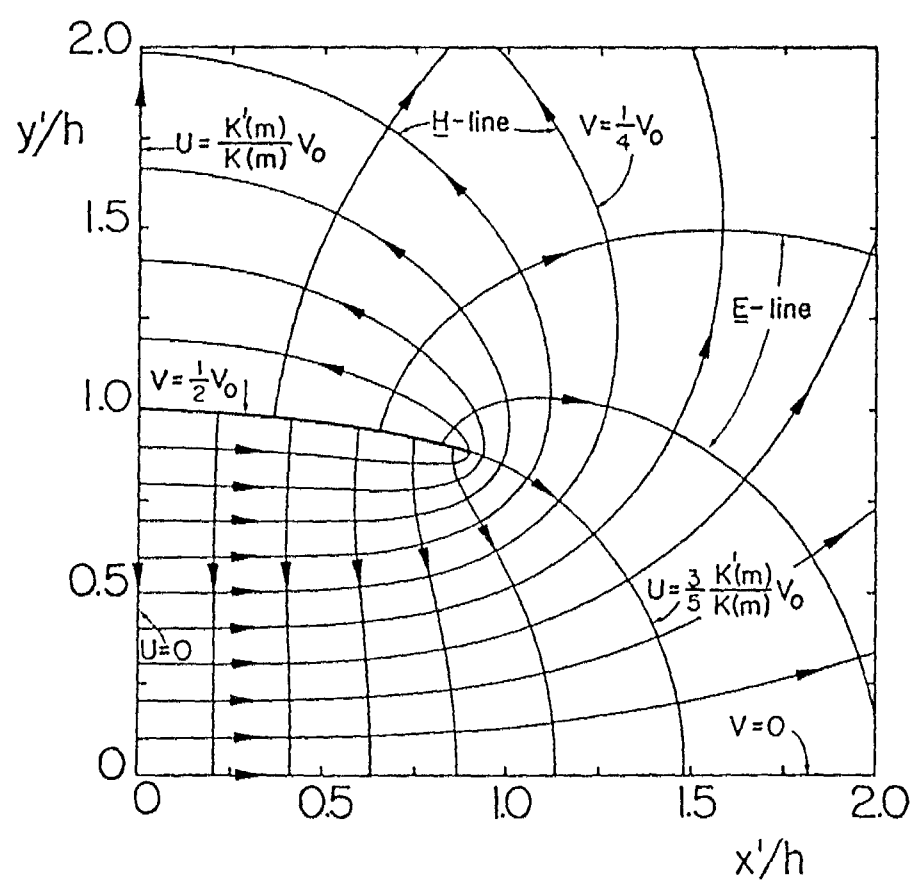

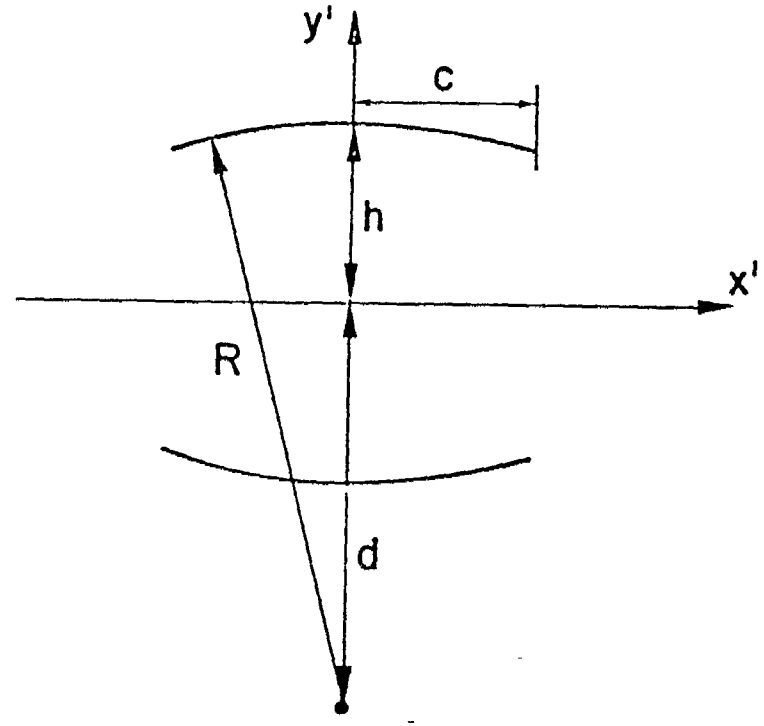

R = 3.41h c = 0.88 h d = 2.41h

Figure 7a. Field lines of the TEM mode for R = 3.41 h , c = 0.88 h , and d = 2.41 h . The characteristic impedance of the transmission line Z_c is 183.9 Ω .

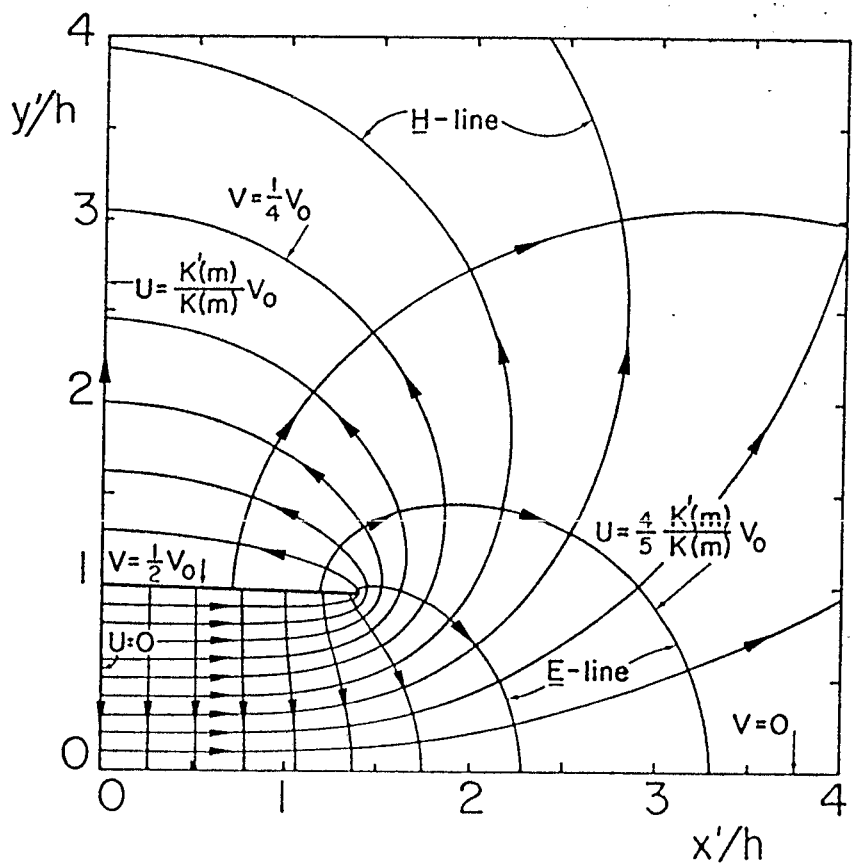

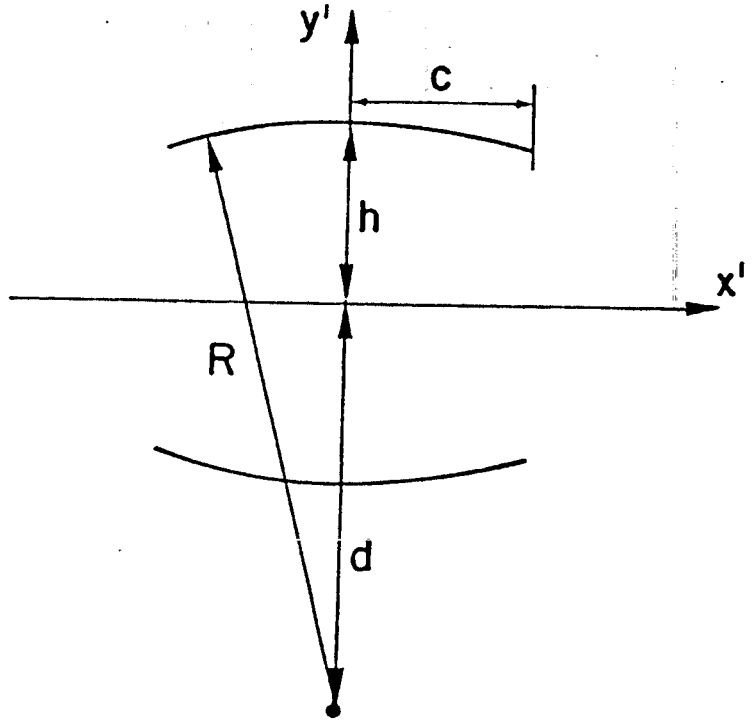

R = 31.91 h c = 1.39 h d = 30.91 h

Figure 7b. Field lines of the TEM mode for R = 31.91 h , c = 1.39 h , and d = 30.91 h. The characteristic impedance of the transmission line Z_c is 145.5 Ω .

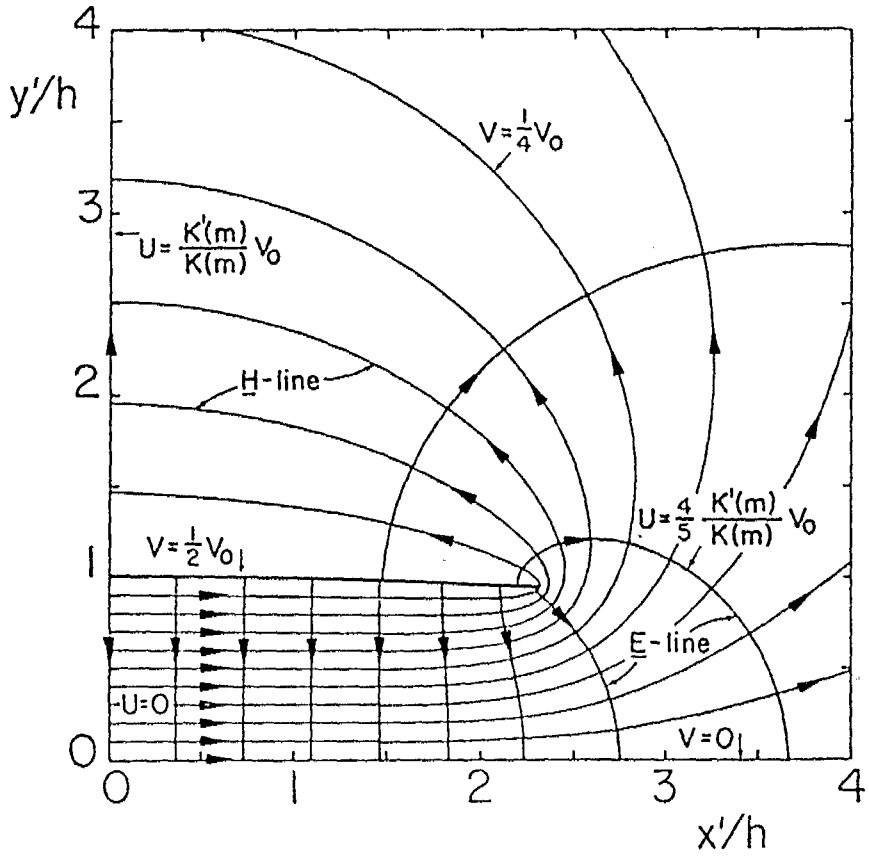

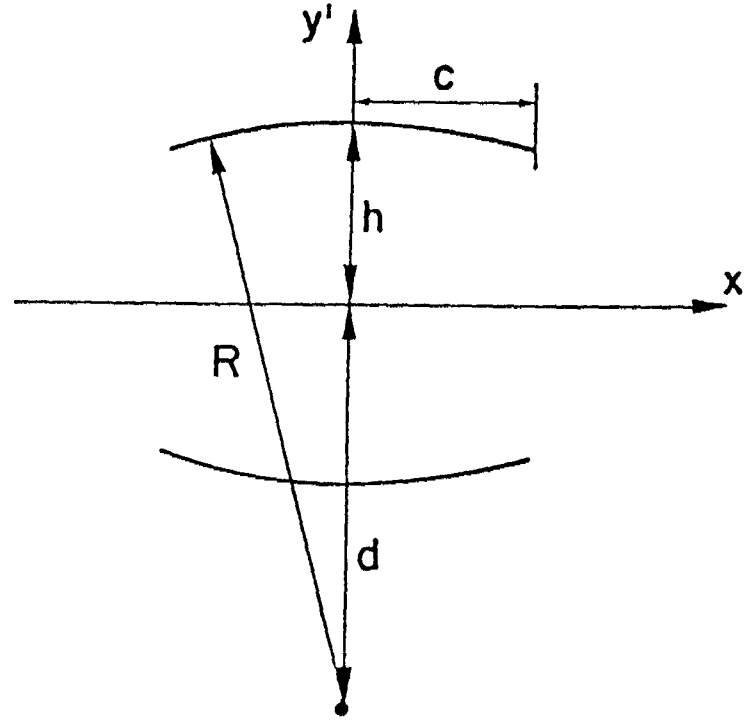

R = 51.50 h c = 2.31 h d = 50.50 h

Figure 7c. Field lines of the TEM mode for R = 51.50 h , c = 2.31 h , and d = 50.50 h . The characteristic impedance of the transmission line Z_c is 102.8 Ω .

It is easy to see that dW/dz' is a real function along the x' and y' axes. Thus, the only nonvanishing field components along these axes are E'_y and H'_x and these quantities are proportional to each other with the proportionality constant Z_o. At the center point $z' = 0$ we have

$$\underline{E}' = - \frac{A_1\sqrt{n}\,(1+\sqrt{n/m})}{(1+\sqrt{n/m}\ - A_1)\sqrt{(1-n)(m-n)}\ K'(m)} \frac{2h}{\sqrt{R^2-d^2}} \frac{V_o}{2h}\hat{y}$$

$$\equiv - E'_o\hat{y} \tag{4}$$

$$\underline{H}' = (E'_o/Z_o)\hat{x}$$

The variation along the x' axis of E'_y (and H'_x) is shown in figure 8. We notice from these curves how the field strength rapidly decreases for $x' > c$. This fact can also be observed from the graph of the field lines in figure 7.

The variation along the y' axis of E'_y (and H'_x) is shown in figure 9. The discontinuity of these quantities at $y' = h$ is proportional to the charge (current) density of the TEM mode at the center of the curved plate.

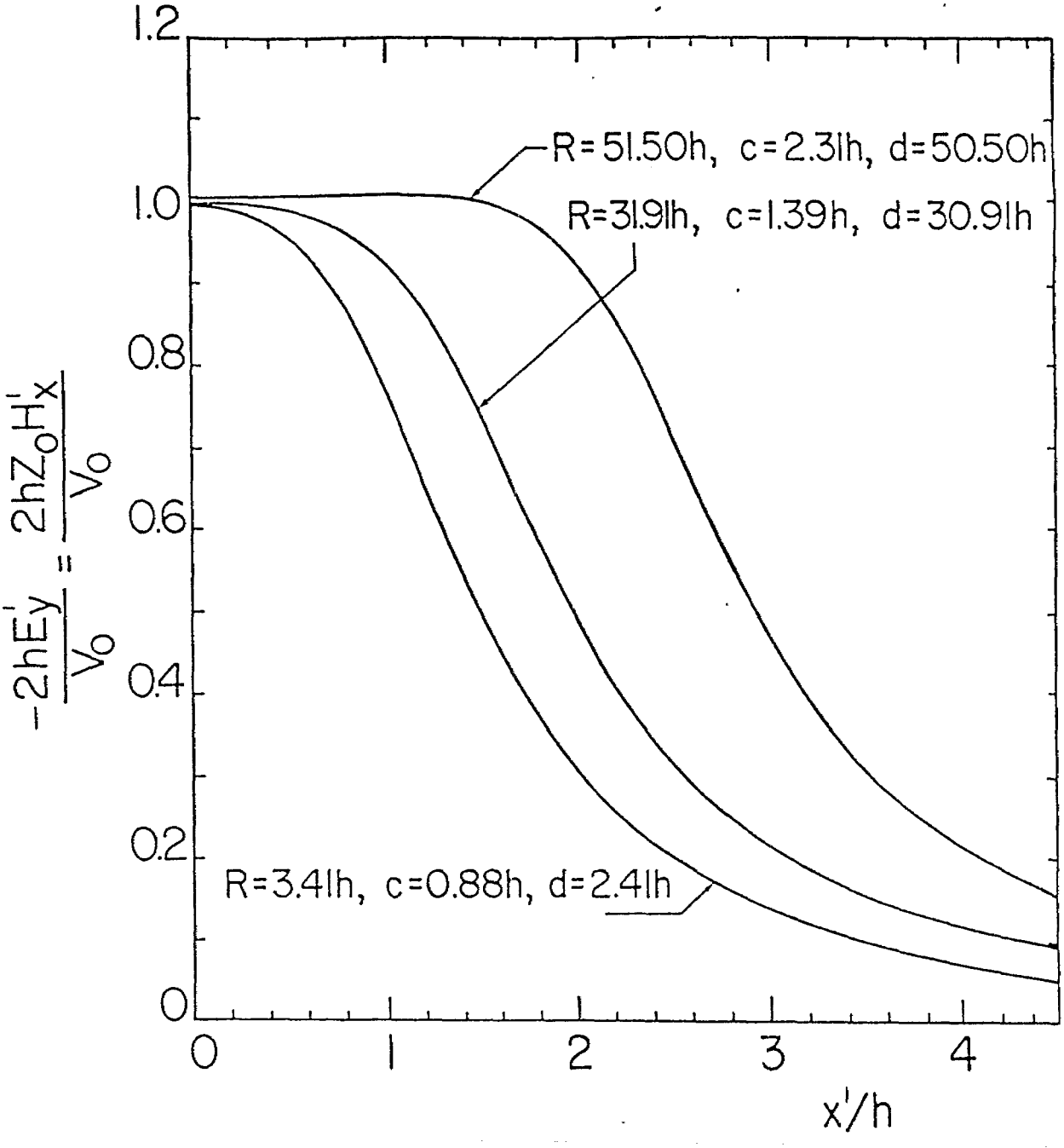

Figure 8. Field variation of the TEM mode along the x' axis.

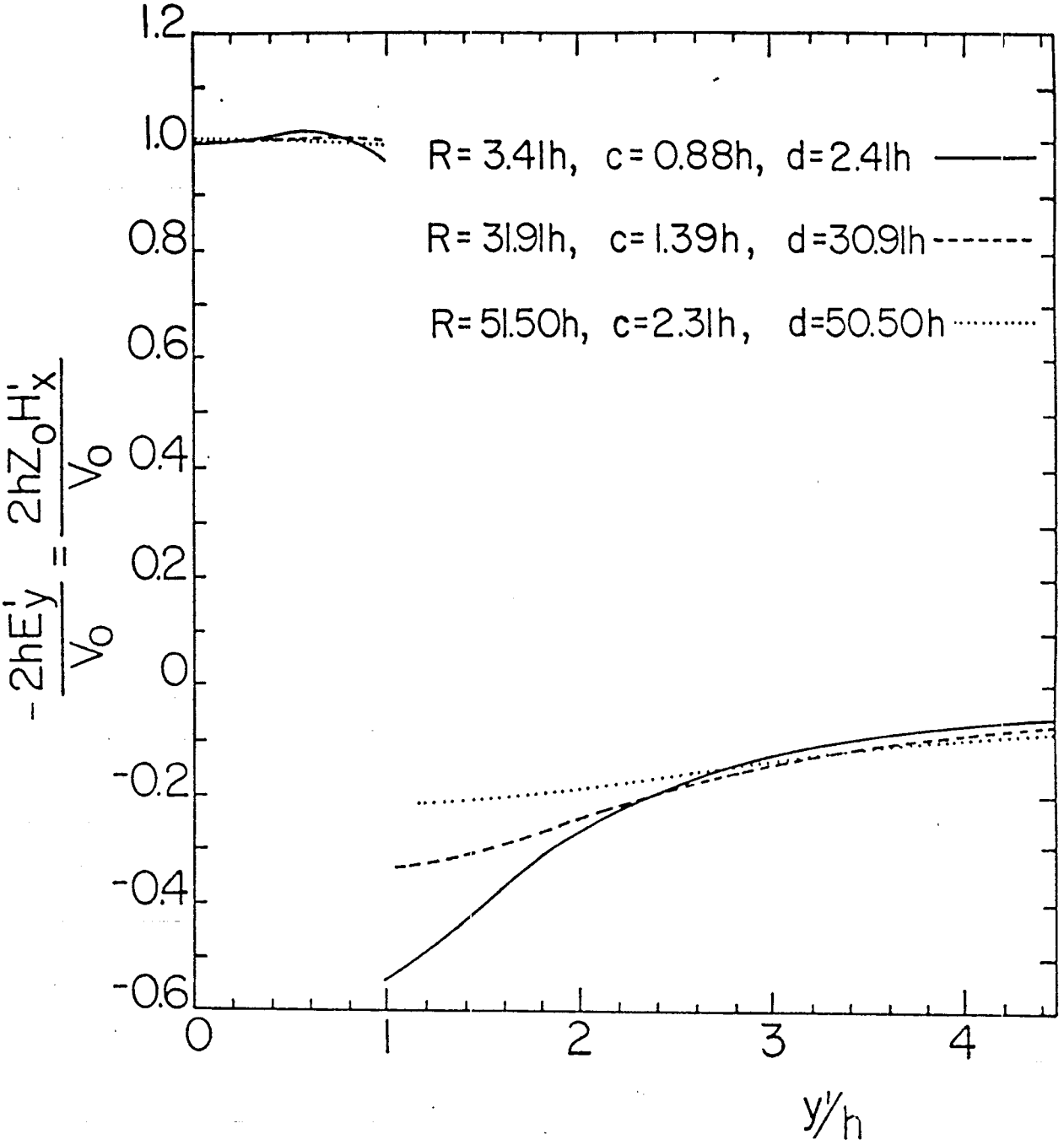

Figure 9. Field variation of the TEM mode along the y' axis.

SECTION IV

TEM-MODE FIELD DISTRIBUTION ON TWO CONICAL PLATES

The field components of the outgoing TEM mode on two conical plates can be expressed in the following manner:

$$\begin{aligned} \underline{E}(\underline{r}) &= \underline{E}(r,\theta,\phi) = \underline{E}(\theta,\phi)\exp(ikr)/r \\ \underline{H}(\underline{r}) &= \hat{r} \times \underline{E}(\underline{r})/Z_o \end{aligned} \tag{5}$$

where (r,θ,ϕ) are spherical coordinates as shown in figure 3. It is obvious that $\underline{E}(\theta,\phi)$ can be obtained from the gradient of the potential function in the following manner

$$\underline{E}(\theta,\phi) = -\frac{\partial V}{\partial \theta}\hat{\theta} - \csc\theta \frac{\partial V}{\partial \theta}\hat{\phi} \tag{6}$$

where V is the imaginary part of the complex potential function $W(z')$. But from the definition of the stereographic projection we have the following relationship:

$$\begin{aligned} x' &= 2\ell \tan(\theta/2)\cos\phi \\ y' &= 2\ell \tan(\theta/2)\sin\phi \end{aligned} \tag{7}$$

so that with the chain rule we have

$$\begin{aligned} \underline{E}(\theta,\phi) &= -\frac{\partial V}{\partial \theta}\hat{\theta} - \csc\theta \frac{\partial V}{\partial \phi}\hat{\phi} \\ &= -\left[\frac{\partial V}{\partial x'}\frac{\partial x'}{\partial \theta} + \frac{\partial V}{\partial y'}\frac{\partial y'}{\partial \theta}\right]\hat{\theta} - \csc\theta\left[\frac{\partial V}{\partial x'}\frac{\partial x'}{\partial \phi} + \frac{\partial V}{\partial y'}\frac{\partial y'}{\partial \phi}\right]\hat{\phi} \\ &= \ell \sec^2(\theta/2)[\cos\phi\, E'_x + \sin\phi\, E'_y]\hat{\theta} \\ &\quad -\ell \sec^2(\theta/2)[\sin\phi\, E'_x - \cos\phi\, E'_y]\hat{\phi} \end{aligned} \tag{8}$$

Here, $\underline{E}' = \underline{E}'(x',y')$ is the field distribution on the curved plates determined in section III. With matrix notation we have ref. 7.

$$\underline{E}(\theta,\phi) = \begin{pmatrix} E_\theta(\theta,\phi) \\ \\ E_\phi(\theta,\phi) \end{pmatrix} = \mathcal{L}_s \cdot \begin{pmatrix} E'_x(x',y') \\ \\ E'_y(x',y') \end{pmatrix} = \mathcal{L}_s \cdot \underline{E}'(x',y') \tag{9}$$

where

$$\mathcal{L}_s = \ell \sec^2(\theta/2) \begin{pmatrix} \cos\phi & \sin\phi \\ \\ -\sin\phi & \cos\phi \end{pmatrix}$$

To sum up, we have the following relationships

$$\begin{aligned} \underline{E}(r) &= \mathcal{L}_s \cdot \underline{E}'(x',y') \exp(ikr)/r \\ \\ \underline{H}(r) &= \mathcal{L}_s \cdot \underline{H}'(x',y') \exp(ikr)/r \end{aligned} \tag{10}$$

Expression (10) gives the field components in a spherical coordinate system which is the natural coordinate system for the two conical plates. But the conical plates are only used as a feed and termination for the two parallel plates between which most of the testing of various objects occurs. The natural coordinate system for the two parallel plates is the rectangular coordinate system. To make the results of this report useful when determining the excitation of the electromagnetic field on two parallel plates we will therefore consider the TEM mode field distribution of the conical plates on the $z = \ell$ plane.

To determine the electric and magnetic fields at the point (x,y,ℓ) in the $z = \ell$ plane we first express the field in rectangular components

$$\begin{aligned}\underline{E}(x,y,\ell) &= \underline{E}(\theta,\phi)\exp(ikr)/r \\ &= \{[\cos\theta\cos\phi\,\hat{\theta}\cdot\underline{E}(\theta,\phi) - \sin\phi\,\hat{\phi}\cdot\underline{E}(\theta,\phi)]\hat{x} \\ &\quad + [\cos\theta\sin\phi\,\hat{\theta}\cdot\underline{E}(\theta,\phi) + \cos\phi\,\hat{\phi}\cdot\underline{E}(\theta,\phi)]\hat{y} \\ &\quad - \sin\theta\,\hat{\theta}\cdot\underline{E}(\theta,\phi)\hat{z}\}\exp(ikr)/r\end{aligned} \tag{11}$$

Using matrix notation

$$\underline{E}(x,y,\ell) = \begin{pmatrix} E_x(x,y,\ell) \\ E_y(x,y,\ell) \\ E_z(x,y,\ell)\end{pmatrix} = \mathcal{L}_c \cdot \begin{pmatrix} E_\theta(\theta,\phi) \\ E_\phi(\theta,\phi)\end{pmatrix} = \mathcal{L}_c \cdot \mathcal{L}_s \cdot \underline{E}'(x',y') \tag{12}$$

where

$$\mathcal{L}_c = \frac{\exp(ikr)}{r}\begin{pmatrix} \cos\theta\cos\phi & -\sin\phi \\ \cos\theta\sin\phi & \cos\phi \\ -\sin\theta & 0\end{pmatrix}$$

and

$$r = (x^2+y^2+\ell^2)^{\frac{1}{2}}\ , \quad \theta = \arccos(\ell/r)\ , \quad \phi = \arctan(y/x)\ .$$

Thus, we have the following relationship between the field components of the TEM mode on the curved plates in the x',y' plane and the field components of the TEM mode on the conical plates in the $z = \ell$ plane

$$\begin{aligned}\underline{E}(x,y,\ell) &= \mathcal{L}_c \cdot \mathcal{L}_s \cdot \underline{E}'(x',y') \\ \underline{H}(x,y,\ell) &= \mathcal{L}_c \cdot \mathcal{L}_s \cdot \underline{H}'(x',y')\end{aligned} \tag{13}$$

The only nonvanishing field components along the x-axis are E_y, H_x, and H_z whereas the only nonvanishing field components along the y-axis are E_y,

E_z , and H_x . In figure 10 we show the strengths of E_y , H_x , and H_z along the x-axis. The phase factor $\exp(ikr)$ (whose magnitude is unity) has been suppressed in these figures and so the quantities displayed are $E_y\exp(-ikr)$ etc. We notice how the field is mainly concentrated to the region between the conical plates. Figure 11 shows the variation of E_y , E_z , and H_x along the y-axis. The discontinuities in these curves occur at the location of the plate and are proportional to the charge and current densities at the center of the plate.

A more detailed description of the field on the conical waveguide is beyond the scope of this report. It is expected, however, that this detailed description will be the topic of a future report.

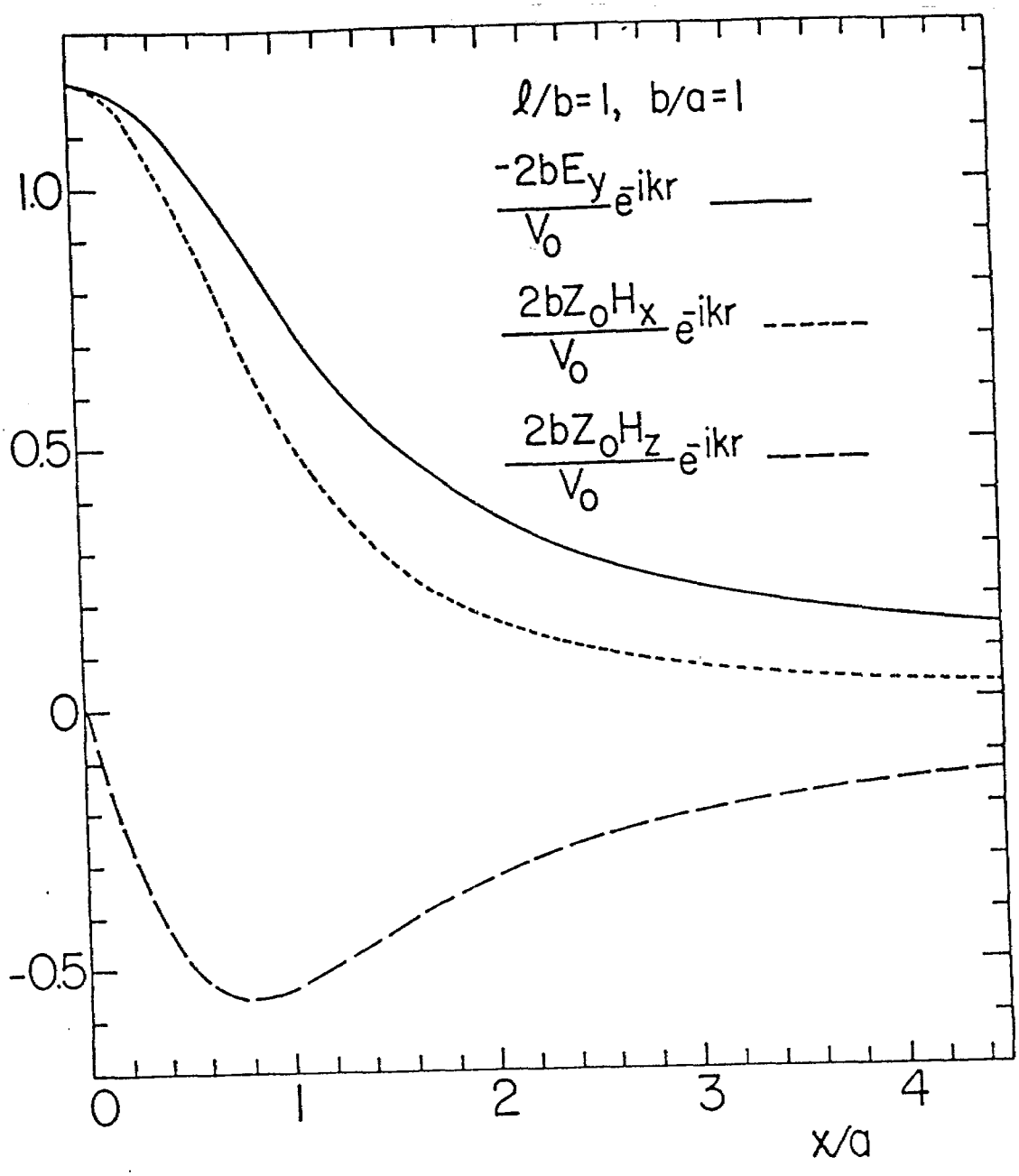

Figure 10a. Field variation of the TEM mode along the x-axis for $\ell/b = 1$ and $b/a = 1$.

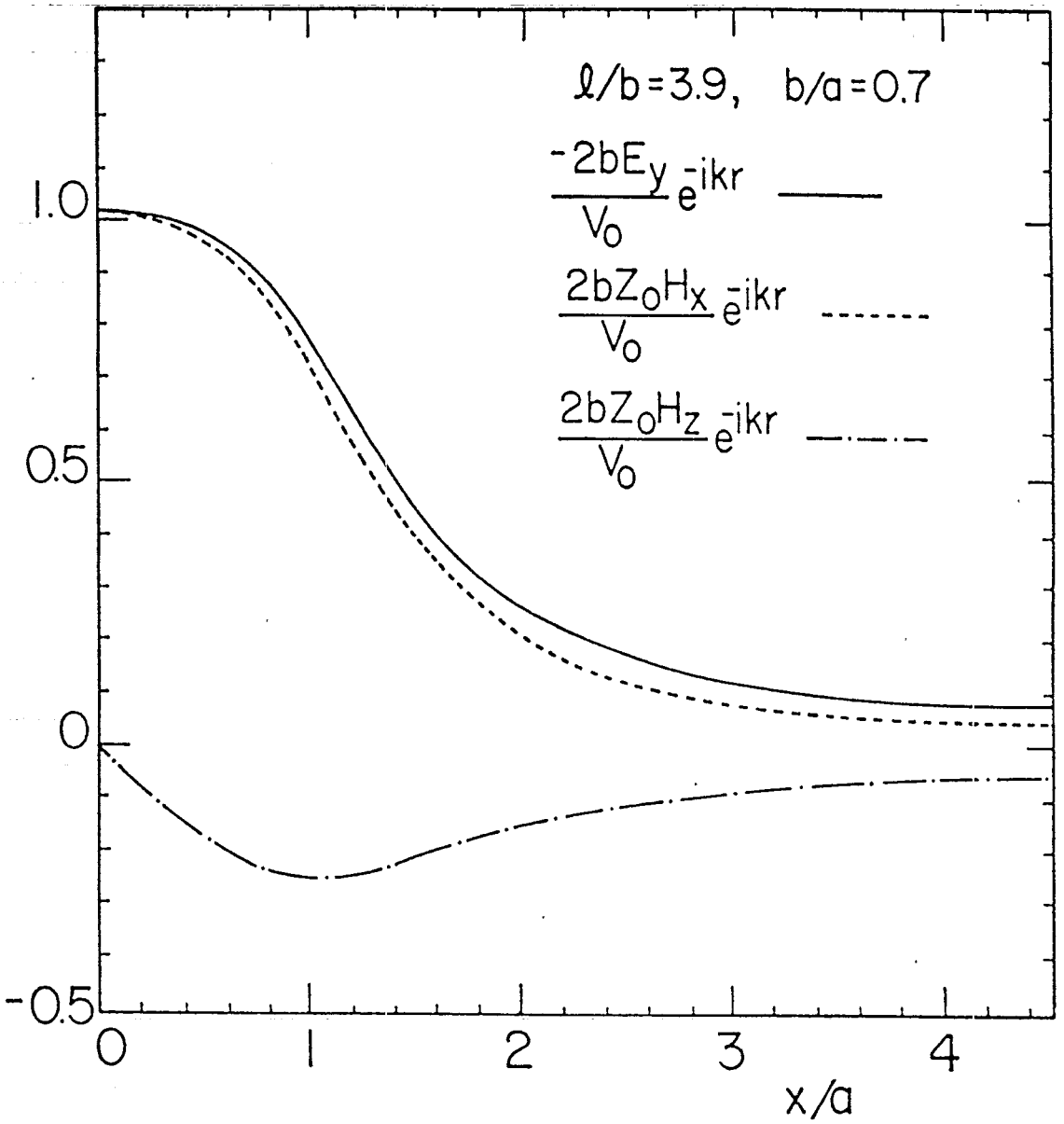

Figure 10b. Field variation of the TEM mode along the x-axis for $\ell/b = 3.9$ and $b/a = 0.7$.

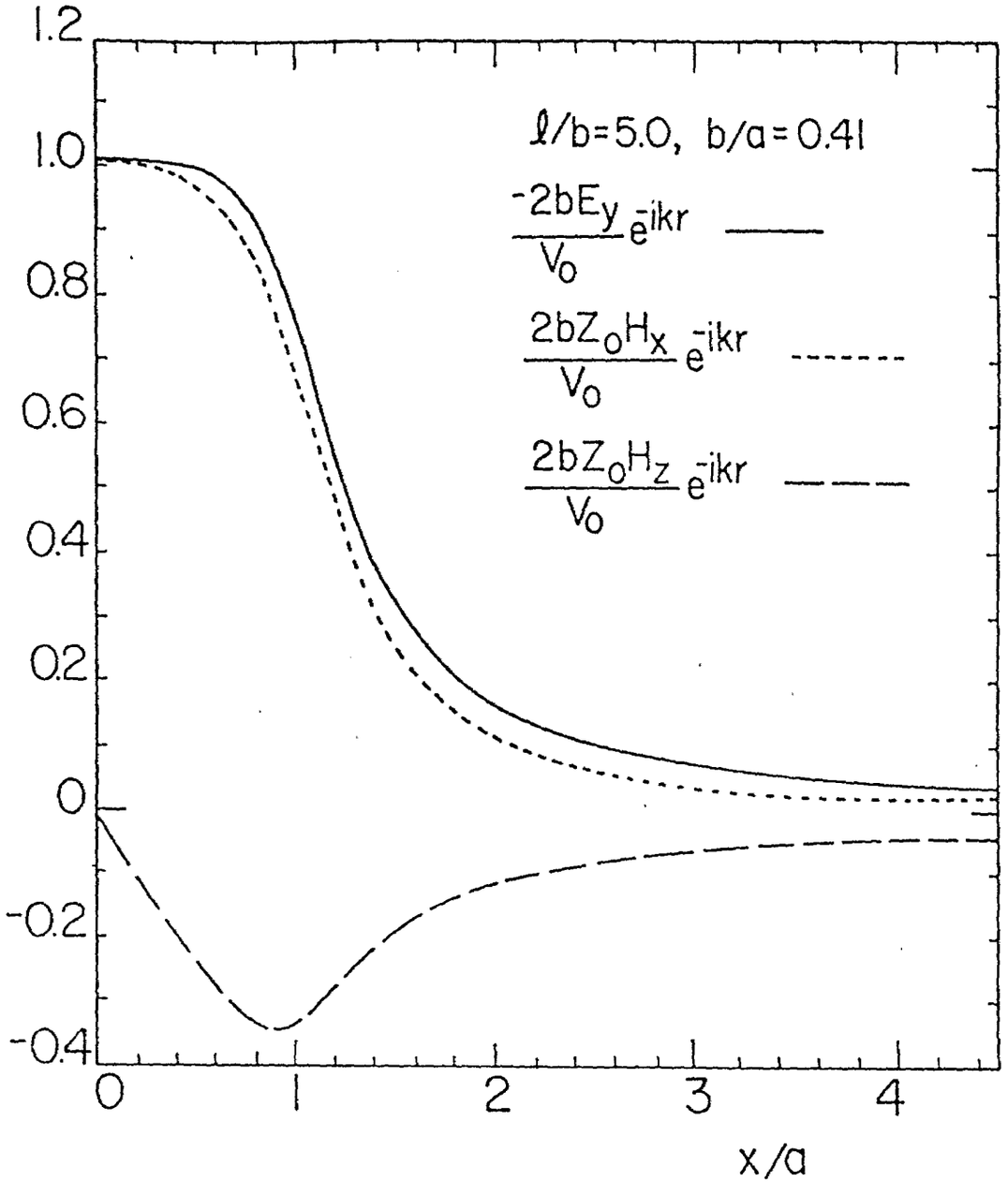

Figure 10c. Field variation of the TEM mode along the x-axis for $\ell/b = 5.0$ and $b/a = 0.41$.

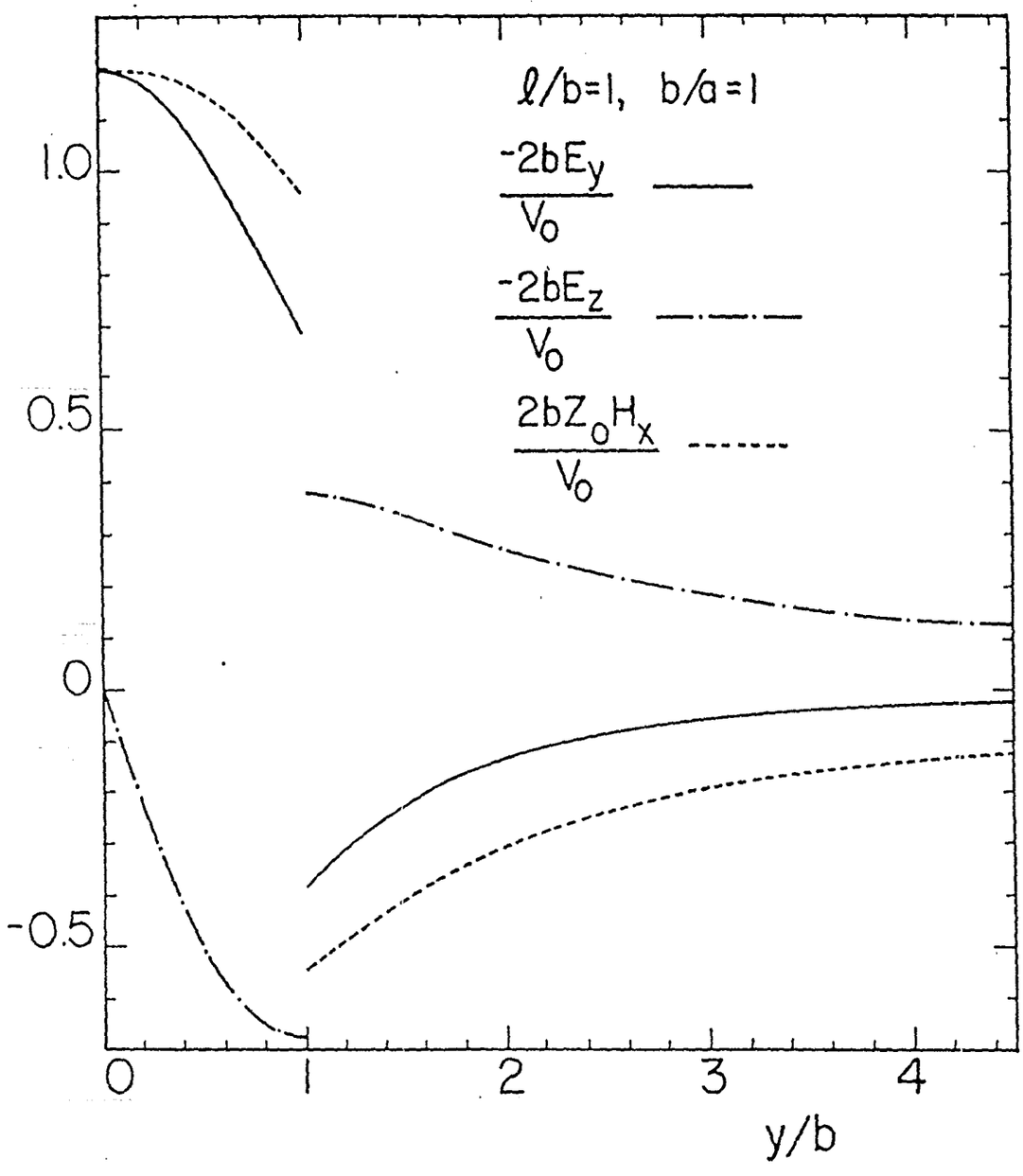

Figure 11a. Field variation of the TEM mode along the y-axis for $\ell/b = 1$ and $b/a = 1$.

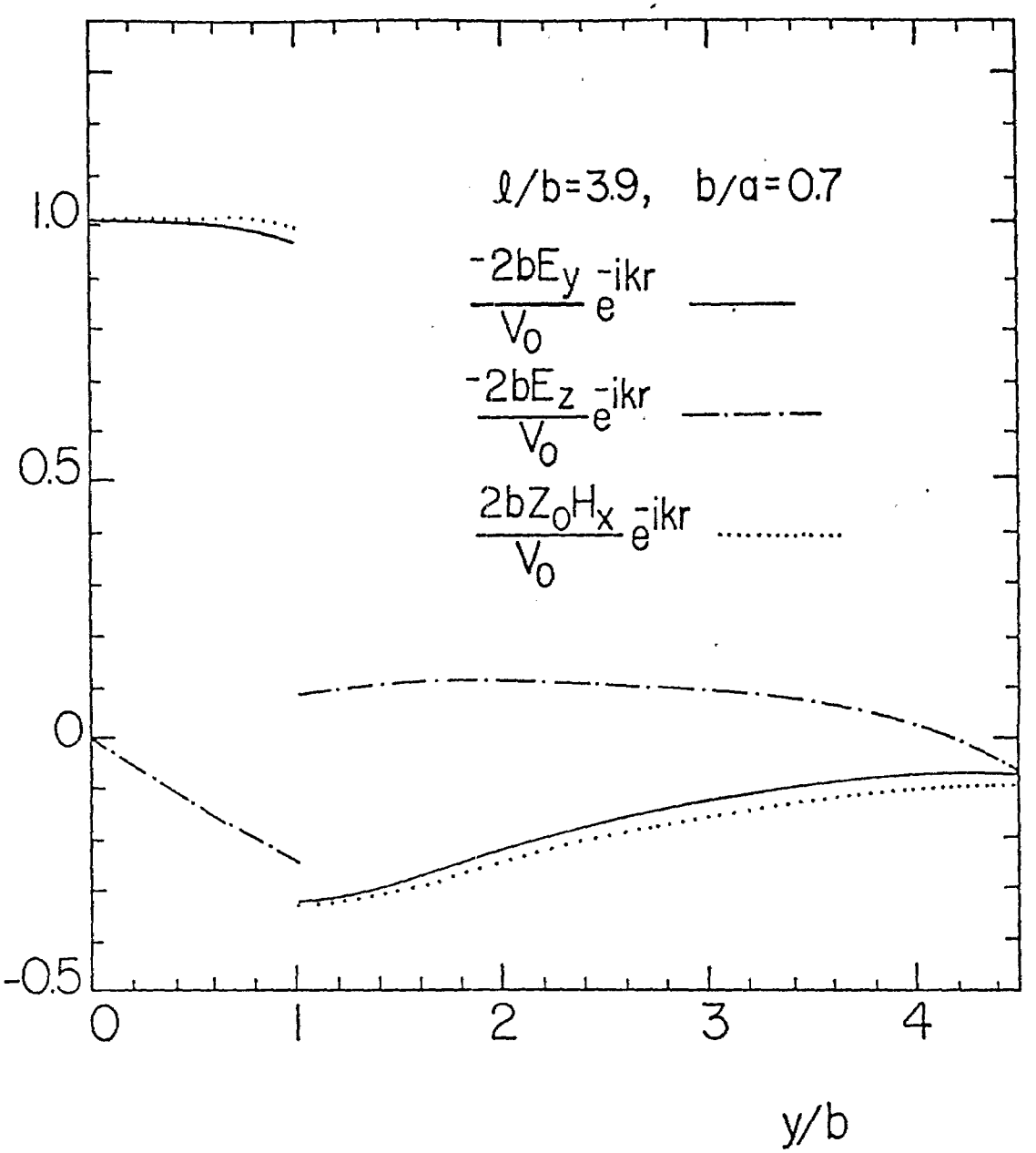

Figure 11b. Field variation of the TEM mode along the y-axis for $\ell/b = 3.9$ and $b/a = 0.7$.

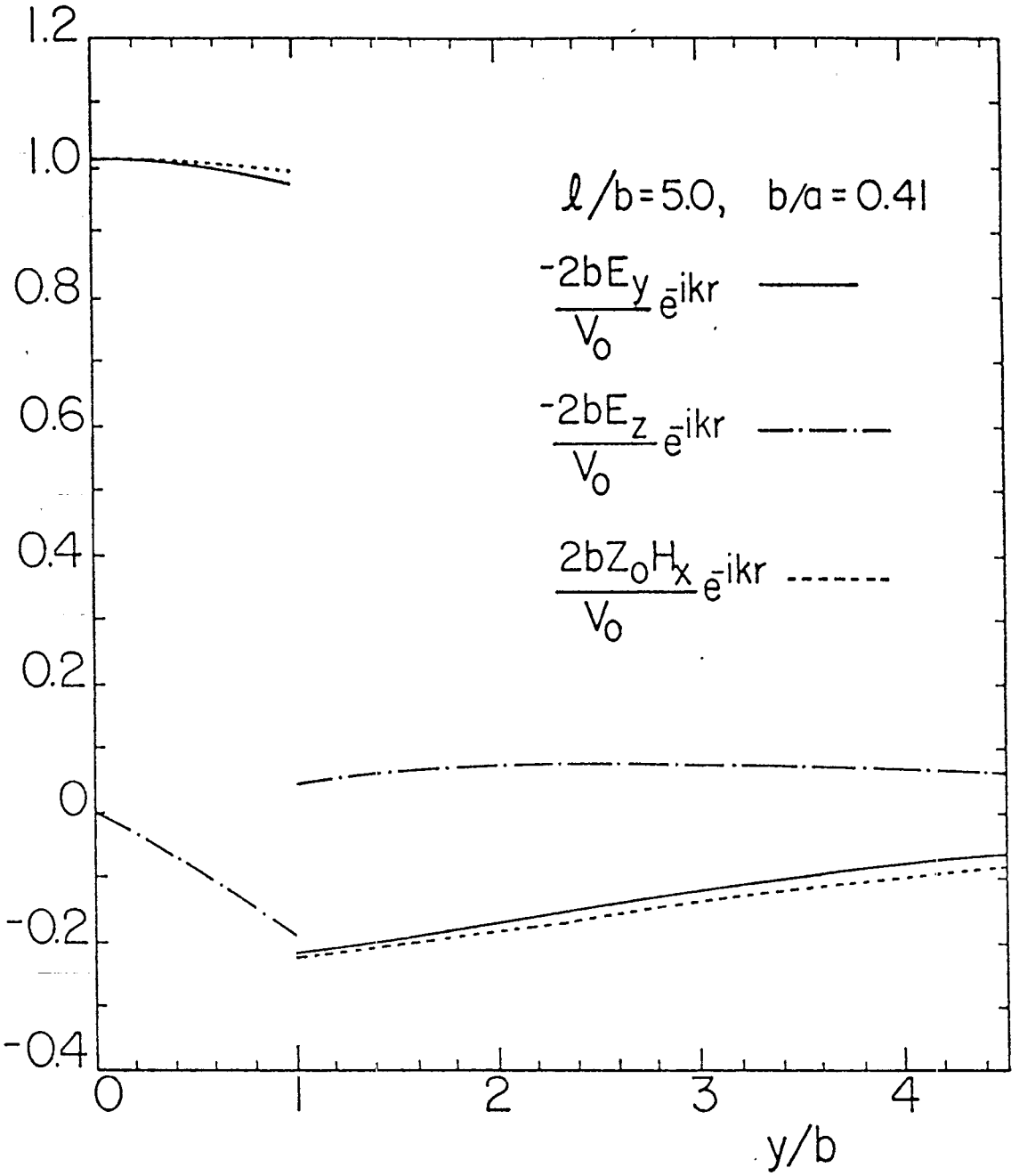

Figure 11c. Field variation of the TEM mode along the y-axis for $\ell/b = 5.0$ and $b/a = 0.41$.

REFERENCES

[1] C.E. Baum, "Impedances and Field Distributions for Parallel-Plate Transmission Lines," Sensor and Simulation Note 21, June 1966.

[2] T.L. Brown and K.D. Granzow, "A Parameter Study of Two Parallel Plate Transmission Line Simulators of EMP Sensor and Simulation Note 21," Sensor and Simulation Note 58, April 1968.

[3] C.E. Baum, D.V. Giri, and R.D. González, "Electromagnetic Field Distribution of the TEM Mode on a Symmetrical Two-Parallel-Plate Transmission Line," Sensor and Simulation Note 219, April 1976.

[4] A.E.H. Love, "Some Electrostatic Distributions in Two Dimensions," Proc. London Math. Soc., Vol. 22, pp. 337 - 369, 1923.

[5] F.C. Yang and K.S.H. Lee, "Impedance of a Two-Conical-Plate Transmission Line," Sensor and Simulation Note 221, November 1976.

[6] C.E. Baum, "A Conical-Transmission-Line Gap for a Cylindrical Loop," Sensor and Simulation Note 42, May 1967.

[7] C.E. Baum, "Early Time Performance at Large Distances of Periodic Planar Arrays of Planar Bicones with Sources Triggered in a Plane-Wave Sequence," Sensor and Simulation Note 184, August 1973.

[8] C.E. Baum, "The Conical Transmission Line as a Wave Launcher and Terminator for a Cylindrical Transmission Line," Sensor and Simulation Note 31, January 1967.

[9] C.E. Baum, "General Principles for the Design of ATLAS I and II. Part V: Some Approximate Figures of Merit for Comparing the Waveforms Launched by Imperfect Pulser Arrays onto TEM Transmission Lines," Sensor and Simulation Note 148, May 1972.

[10] T.K. Liu, "Impedances and Field Distributions of Curved Parallel-Plate Transmission-Line Simulators," Sensor and Simulation Note 170, February 1973.